J. theor. Biol. (1998) **193,** 1–18
Article No. jt980670

Membrane Binding-site Density Can Modulate Activation Thresholds in Enzyme Systems

AARON L. FOGELSON* AND ANDREW L. KUHARSKY

Department of Mathematics, University of Utah, Salt Lake City, UT 84112, *U.S.A.*

(*Received on* 23 *June* 1997, *Accepted in revised form on* 22 *January* 1998)

The kinetic equations are analysed for a model system which is motivated by the reactions of blood coagulation, and which involves two zymogen–enzyme pairs each of which can exist in solution phase or bound to a membrane. The enzyme of each pair activates the zymogen of the other pair, and each enzyme is subject to first-order inactivation both in solution and when bound to the membrane. If enzyme activation happens exclusively or predominantly in the membrane phase, then the system displays a threshold response which can be modulated by varying the density of membrane binding sites for the zymogens and enzymes. For low densities of membrane binding sites, the system's response when challenged by a dose of enzyme quickly decays away. For high enough densities of membrane binding sites, the system responds with substantial and sustained enzyme production. Thus variations in surface-binding site densities can serve as a "switch", drastically altering the responsiveness of the system. Such a binding-site-mediated switching mechanism could have profound importance to the regulation of enzyme systems, in particular, the blood coagulation system.

1. Introduction

Blood coagulation involves a series of enzymatic reactions, a typical one of which leads to the activation of an inactive plasma zymogen into an active enzyme. The final enzyme in the series is thrombin which cleaves the plasma protein fibrinogen into fibrin monomers. These polymerize and crosslink to form a fibrous mesh that helps give a blood clot its strength. Coagulation was once thought to be a linear sequence or "cascade" with the activated product of one reaction catalysing the next reaction (Davie & Ratnoff, 1964; MacFarlane, 1964), but is now known to also involve feedforward and feedback loops in which an enzyme produced in one step promotes or inhibits earlier or later reactions. Some of the coagulation reactions happen in the plasma, but an apparently critical role is played by *membrane-bound* enzyme complexes. Signal amplification and tight regulation are the presumed reasons for the multitude of steps and the feedback loops, respectively, but, in fact, despite the extreme importance of coagulation in normal hemostasis and in pathological thrombosis, our understanding of its *dynamics* is poor. Not only is the biochemical reaction network itself complex, but coagulation dynamics also depend on the binding of reactants to appropriate phospholipid surfaces (Mann *et al.*, 1990) and on their transport in the plasma by diffusion and flow (Gemmell *et al.*, 1988). Figure 1 shows a schematic of some of the major reactions of the coagulation process. The layout of the figure is intended to emphasize that different reactions occur at distinct spatial locations.

Below we give a brief review of the coagulation reaction system. There are several noteworthy features of this system that one should keep in mind: one is the presence of several positive feedback loops. A second is the upregulation of coagulation inhibitors

*Author to whom correspondence should be addressed.

0022–5193/98/130001 + 18 $30.00/0

by the coagulation enzymes themselves. A third is the apparently critical role played by surface-bound enzyme complexes. The major goal of this paper is to explore in a simple model system how the requirement for surface binding might help regulate the overall behavior of the coagulation system.

1.1. REVIEW OF THE COAGULATION SYSTEM

Coagulation is believed to be initiated when Tissue Factor (TF) molecules embedded in the vessel wall are exposed by injury (Nemerson, 1992) [see Fig. 1(b)] and bind plasma enzyme Factor VIIa. The surface-

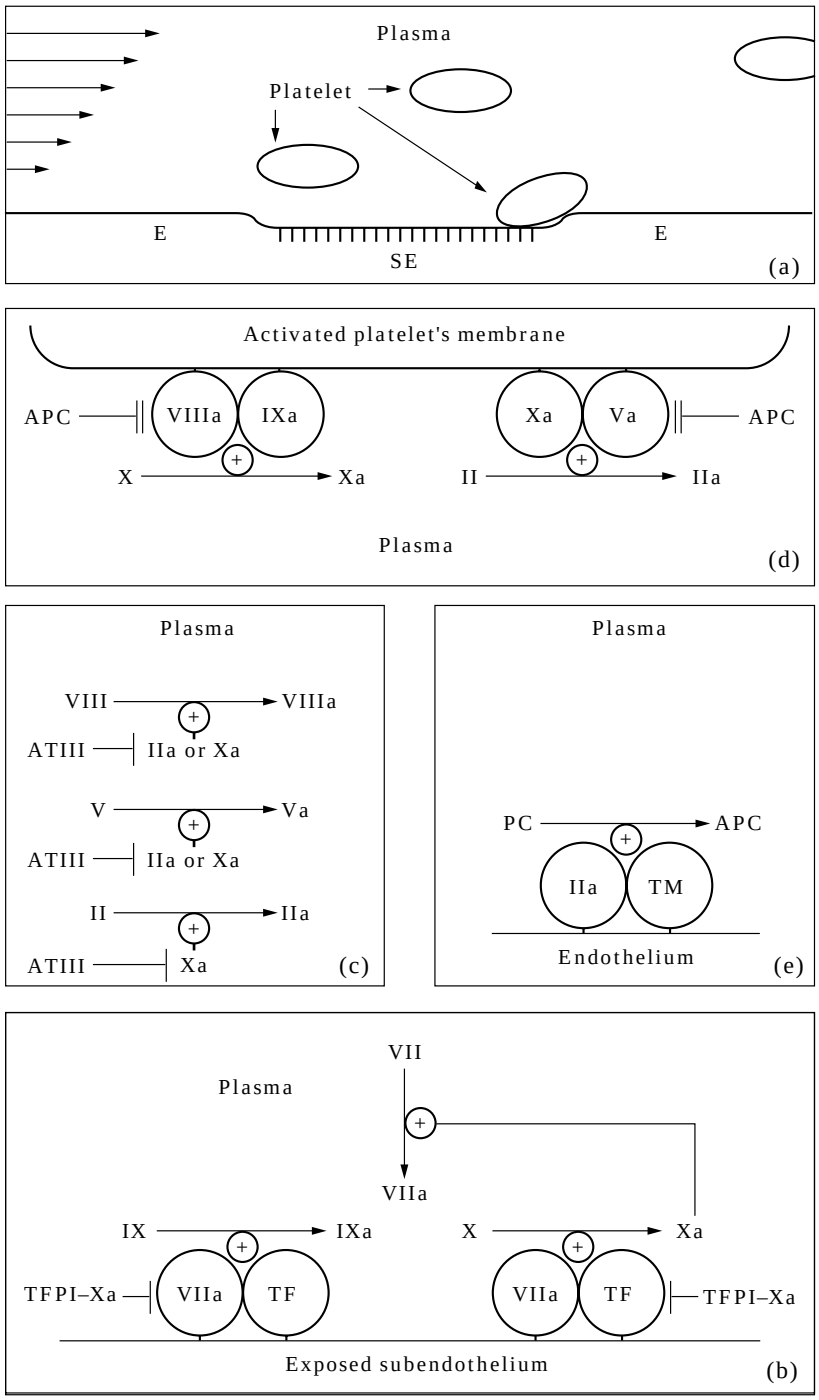

FIG. 1. Coagulation reactions: (a) schematic of injured site. SE—exposed subendothelium, E—endothelium; (b) TF-VIIa system on subendothelium; (c) plasma-phase reactions; (d) VIIIa:IXa and Va:Xa complexes on activated platelet surface; (e) TM:IIa complex on endothelial surface. ⊕ indicates enzymatically-promoted reaction. ⊣ indicates inhibition. ⫤ indicates inactivation.

bound complex TF:VIIa activates plasma zymogen Factors IX and X into enzymes IXa and Xa (Nemerson, 1992; Silverberg *et al*., 1977; Zur & Nemerson, 1980; Krishnaswamy *et al*., 1992). Activated Factor Xa in turn is a potent activator of Factor VII into enzyme VIIa (Radcliffe & Nemerson, 1976); this is our first example of a surface-dependent positive feedback loop. Factor Xa also activates plasma zymogen Factors V and VIII into Va and VIIIa and each of these can then serve as the *anchor* for a membrane-bound enzyme complex (VIIIa:IXa and Va:Xa) on the surface of an *activated* platelet [see Fig. 1(d)] (Krishnaswamy *et al*., 1993; Mann *et al*., 1990). The platelet-bound VIIIa:IXa complex activates Xa; Xa binds with Va on a platelet's surface to form the Va:Xa or prothrombinase complex which activates prothrombin (Factor II) into thrombin (Factor IIa). While plasma-phase Factor Xa is a weak activator of prothrombin into thrombin (Mann & Lorand, 1993; Rosing *et al*., 1980) [see Fig. 1(c)], the platelet-bound Va:Xa complex is a *very potent* thrombin activator; its effectiveness is 5 *orders of magnitude greater* (Miletich *et al*., 1977) than that of plasma-phase Xa and thus is likely the dominant source of thrombin activation.

The formation and activity of the VIIIa:IXa and Va:Xa complexes is critically dependent on the availability of suitable phospholipid binding sites; these sites are not present on normally circulating platelets, but are present on activated platelets. Platelet activation can be induced by direct contact of platelets with collagens exposed in the injured vessel tissue, by the action of thrombin, or by other platelet-secreted plasma-phase chemical messengers like adenosine diphosphate (ADP).

Thrombin is the final enzyme produced by the coagulation cascade, and it plays several roles in coagulation. As mentioned above, it promotes the formation of a fibrin mesh and this mechanically stabilizes the platelet aggregates which have formed on the injured vessel. Thrombin also promotes its own production by activating factors V and VIII and by activating platelets (Nesheim & Mann, 1979; Monkovic & Tracy, 1990; Lollar *et al*., 1985; Eaton *et al*., 1986). Thrombin plays at least one more, and quite different, role in coagulation. Thrombin binds with thrombomodulin (TM) which is located on the surface of the endothelial cells that line the undamaged vessel wall [see Fig. 1(e)]. This has two effects: (1) the bound thrombin is inhibited in its procoagulant role, and (2) the TM–thrombin complex activates plasma Protein C into Activated Protein C (APC). APC is a potent anti-coagulant which cleaves Factors VIIIa and Va thus inactivating them and preventing their serving as cofactors in the VIIIa:IXa and Va:Xa complexes [see Fig.1(b)] (Esmon, 1989). Two other major inhibitors of coagulation are Antithrombin III (ATIII) and Tissue Factor Pathway Inhibitor (TFPI). ATIII competitively inhibits Factor Xa and thrombin [see Fig. 1(c)] (Bauer & Rosenberg, 1987), while TFPI binds with Factor Xa to inhibit the activity of the TF-VIIa complex (Pedersen *et al*., 1990; Broze *et al*., 1990; Rapaport, 1989) and to block the activity of the Factor Xa that is bound to TFPI. Excellent reviews of the coagulation pathways can be found in Mann *et al*. (1990) and Hemker & Kessels (1991).

1.2. PREVIOUS MODELS

A number of research groups have recognized the usefulness of mathematical modeling in trying to understand the coagulation process. Nesheim *et al*. (1984, 1992) explore a steady-state model of prothrombinase activity. The model involves two phases, one corresponding to the bulk solution, and the other to thin shells surrounding phospholipid membranes. The two phases are colocalized in that the model includes no explicit spatial dependencies. The model includes a single substrate, prothrombin, which can exist either in the bulk solution or bound to the membrane (in the "shells"), as well as a solution-phase enzyme, Factor Xa, and a surface-bound enzyme complex, prothrombinase (Va:Xa), each of which activate prothrombin to thrombin. The distribution of substrate and enzyme Factor Xa between the two phases is assumed to be in equilibrium and determined solely by surface binding parameters and the prescribed total concentrations of phospholipid, substrate, and enzyme. The steady-state rate of thrombin production in both phases is examined as a function of phospholipid concentration, other kinetic parameters, and assumptions about whether substrate and enzyme have specific membrane binding sites or compete for the same sites. More recent modeling from the same laboratory (Jones & Mann, 1994) looks at dynamic interactions among a number of the coagulation enzymes and zymogens. These new models ignore inhibition and, importantly, assume a great excess of phospholipid, and therefore do not address the possible regulatory role played by phospholipid surfaces in controlling the coagulation reactions. Willems *et al*. (1991) study a dynamic model of thrombin production in plasma, allowing for inhibition by APC and exogenous hirudin. The stimulus in the system is a brief pulse of Factor Xa, and a threshold response to this stimulus is reported. The model inputs include phospholipid concentration, but the effect of this concentration

TABLE 1
The three model scenarios

Scenario	Major assumptions
1	Spatially homogeneous; enzyme activation on membrane only
2	Spatially homogeneous; enzyme activation on membrane and in solution
3	Spatially inhomogeneous; enzyme activation on membrane only

on system behavior is not reported. Jesty *et al*. (1993) take a different tack in analysing a model two-zymogen two-enzyme positive feedback loop with inhibition which they think extracts some of the essential features of the coagulation reactions without matching exactly any part of the coagulation pathway. In their system, zymogen Z_1 can be activated by enzyme E_2 to produce enzyme E_1. Enzyme E_1 in turn activates zymogen Z_2 to enzyme E_2. Both enzymes are subject to first order inactivation. Their main result is that the system has a threshold. If the product of activation rates is less than the product of inactivation rates, then the system's response to a stimulus (an increment of enzyme) quickly decays. If the product of activation rates exceeds the product of inactivation rates, the same stimulus produces a large conversion of zymogen to enzyme. In Beltrami & Jesty (1995) this analysis is extended to larger systems made up of multiple interacting feedback loops. The results of this approach are interesting but are limited in that the analysis is for solution-phase reactions only; no account is taken of surface binding or transport of reactants to and from reactive surfaces even though surface reactions seem to play a major regulatory role in coagulation.

In this paper, we consider an extension of the Jesty–Beltrami approach which includes both solution-phase and membrane-phase reactions. We consider dynamic models (not just steady state), we do not assume that instantaneous binding equilibria are established between the phases, and in some of our analysis we consider the effect of finite-rate diffusion between the two phases, In our models, the concentrations of membrane binding-sites are limited and we treat them as control variables.

2. Model Systems

We consider three scenarios for zymogen–enzyme interactions that involve membrane and solution phases. Each scenario involves two zymogen–enzyme pairs. In the solution phase these are denoted Z_1, E_1 and Z_2, E_2, respectively; when bound to receptors on the membrane they are denoted Z_1^m, E_1^m and Z_2^m, E_2^m. The concentration or density of each of these species is denoted in a similar way but with lower-case z or e. In the first scenario, each membrane-bound enzyme catalyses the activation of the membrane-bound zymogen corresponding to the other enzyme, while the solution-phase enzymes are assumed to have negligible activity. In the second scenario, the solution-phase enzymes are also assumed to be active and able to activate the solution-phase zymogen corresponding to the other enzyme. In both of these scenarios, diffusion within the solution to the membrane is assumed to be extremely rapid, i.e. any limitations due to diffusion are ignored. The third scenario involves the same reactions as the first, but accounts for the limitations of finite solution-phase diffusion. Figure 2 shows the reaction networks for the three scenarios and Table 1 summarizes the major assumptions for each scenario. For Scenarios 1 and 3, the rate constants k_{1cat} and k_{2cat} for solution-phase enzyme activation are taken to be zero.

The assumptions which underlie the network in Fig. 2 are as follows: there are two populations of membrane binding sites with total (surface) densities r_1^T and r_2^T. Zymogen Z_1 and enzyme E_1 can bind to membrane binding sites of type 1; Z_2 and E_2 can bind to binding sites of type 2. The rate of binding of Z_1 or E_1 to membrane binding sites is proportional to the density of *unoccupied* binding sites of type 1, $r_1 \equiv r_1^T - e_1^m - z_1^m$ with second order rate constants k_{1on} and k_{1on}^z for the enzyme E_1 and zymogen Z_1, respectively. The dissociation of E_1^m and Z_1^m from their membrane binding sites is determined by first order rate constants k_{1off} and k_{1off}^z. The binding and dissociation of Z_2 and E_2 are assumed to be governed by similar relations with second order binding rates k_{2on} and k_{2off}^z, free binding-site density $r_2 \equiv r_2^T - e_2^m - z_2^m$, and first order off rates k_{2off} and k_{2off}^z. Enzyme E_1 is assumed to decay (or be inactivated) with first order rate constants k_{1in} in solution and k_{1in}^m on the membrane. The corresponding rate constants for enzyme E_2 are denoted k_{2in} and k_{2in}^m. Each enzyme activates the zymogen of the *other* pair at a rate that obeys Michaelis–Menton kinetics and is therefore described by two parameters, k_{cat} and K_M. There are four sets of these parameters: (k_{1cat}^m, K_{1M}^m), (k_{2cat}^m, K_{2M}^m), (k_{1cat}, K_{1M}), and (k_{2cat}, K_{2M}).

2.1. EQUATIONS FOR SCENARIO 3—SPATIALLY VARYING CASE

The equations for Scenario 3 are the most fundamental, and so we describe them first. In this scenario, the solution-phase concentrations depend on time t and on the distance y from the membrane surface. These concentrations evolve according to the equations:

2.1.1. *Equations in solution*

$$\frac{\partial e_1}{\partial t} = D_1 \frac{\partial^2 e_1}{\partial y^2} + \frac{k_{1cat} e_2 z_1}{K_{1M} + z_1} - k_{1in} e_1 \tag{1}$$

$$\frac{\partial z_1}{\partial t} = D_1 \frac{\partial^2 z_1}{\partial y^2} - \frac{k_{1cat} e_2 z_1}{K_{1M} + z_1} \tag{2}$$

$$\frac{\partial e_2}{\partial t} = D_2 \frac{\partial^2 e_2}{\partial y^2} + \frac{k_{2cat} e_1 z_2}{K_{2M} + z_2} - k_{2in} e_2 \tag{3}$$

$$\frac{\partial z_2}{\partial t} = D_2 \frac{\partial^2 z_2}{\partial y^2} - \frac{k_{2cat} e_1 z_2}{K_{2M} + z_2} \tag{4}$$

where D_1 and D_2 are the diffusion coefficients for the pairs e_1, z_1, and e_2, z_2, respectively. The densities of membrane-bound enzymes and zymogens obey the equations:

2.1.2. *Equations on membrane*

$$\frac{\mathrm{d}e_1^m}{\mathrm{d}t} = k_{1on} e_1 \{r_1^T - e_1^m - z_1^m\} - k_{1off} e_1^m + \frac{k_{1cat}^m e_2^m z_1^m}{K_{1M}^m + z_1^m} - k_{1in}^m e_1^m \tag{5}$$

$$\frac{\mathrm{d}z_1^m}{\mathrm{d}t} = k_{1on}^z z_1 \{r_1^T - e_1^m - z_1^m\} - k_{1off}^z z_1^m - \frac{k_{1cat}^m e_2^m z_1^m}{K_{1M}^m + z_1^m} \tag{6}$$

$$\frac{\mathrm{d}e_2^m}{\mathrm{d}t} = k_{2on} e_2 \{r_2^T - e_2^m - z_2^m\} - k_{2off} e_2^m + \frac{k_{2cat}^m e_1^m z_2^m}{K_{2M}^m + z_2^m} - k_{2in}^m e_2^m \tag{7}$$

$$\frac{\mathrm{d}z_2^m}{\mathrm{d}t} = k_{2on}^z z_2 \{r_3^T - e_2^m - z_2^m\} - k_{2off}^z z_2^m - \frac{k_{2cat}^m e_1^m z_2^m}{K_{2M}^m + z_2^m} \tag{8}$$

Boundary conditions at $y = 0$ connect the solution and membrane phases; they are:

2.1.3. *Equations for solution-membrane interactions*

$$-D_1 \frac{\partial e_1}{\partial y} = k_{1off} e_1^m - k_{1on} e_1 \{r_1^T - e_1^m - z_1^m\} \tag{9}$$

$$-D_1 \frac{\partial z_1}{\partial y} = k_{1off}^z z_1^m - k_{1on}^z z_1 \{r_1^T - e_1^m - z_1^m\} \tag{10}$$

$$-D_2 \frac{\partial e_2}{\partial y} = k_{2off} e_2^m - k_{2on} e_2 \{r_2^T - e_2^m - z_2^m\} \tag{11}$$

$$-D_2 \frac{\partial z_2}{\partial y} = k_{2off}^z z_2^m - k_{2on}^z z_2 \{r_2^T - e_2^m - z_2^m\} \tag{12}$$

These equations describe the balance between the diffusive flux of each species to or from the surface, and its rate of consumption or production on the surface. We also impose boundary condition at a distance $y = y_{max}$ from the membrane; we either fix the species concentrations e_1, z_1, e_2, and z_2 there or specify that there be no flux of these species across $y = y_{max}$.

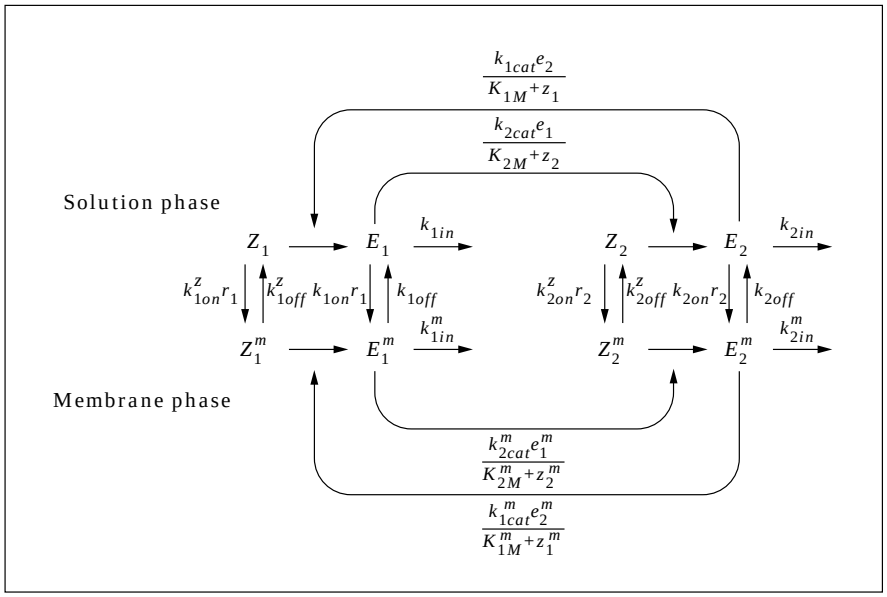

FIG. 2. Enzyme reaction network: model system with two zymogen–enzyme pairs and surface binding.

We must also specify initial conditions for e_1, z_1, e_2, and z_2 for $0 \leqslant y \leqslant y_{max}$, and for e_1^m, z_1^m, e_2^m, and z_2^m.

We note that in the above equations, e_i and z_i have units of moles/volume for $i = 1, 2$; e_i^m and z_i^m have units of moles/area; k_i, k_i^m, k_{icat}^m, k_{icat}, k_{ioff}, and k_{ioff}^z have units of 1/time; k_{ion} and k_{ion}^z have units of 1/((time)(moles/volume)); K_{iM} has units of moles/volume; and K_{iM}^m has units of moles/area. Throughout the paper, we express volume concentrations in nM, first order rate constants in $(s)^{-1}$, second order rate constants in $(nM\ s)^{-1}$, and time in s, but our analysis holds true in any consistent set of concentration, distance, and time units.

2.2. EQUATIONS FOR SCENARIOS 1 AND 2—SPATIALLY HOMOGENEOUS CASE

The equations for Scenarios 1 and 2 are derived from those above by assuming that diffusion is extremely fast and that therefore, in effect, the solution phase and membrane phase are colocalized. Because of this, it is convenient to express all concentrations in moles/volume, rather than expressing surface concentrations in moles/area. To this end, we let γ denote the area of membrane surface per unit volume of solution, and define $e_1^{mv} = \gamma e_1^m$, $z_1^{mv} = \gamma z_1^m$, $r_i^{Tv} = \gamma r_i^T$, and $K_{iM}^{mv} = \gamma K_{iM}^m$, for $i = 1, 2$. Thus, e_1^{mv}, for example, is the number of moles of membrane-bound E_1 per volume of solution. The superscript v is intended as a reminder that these variables are expressed in moles per unit *volume*. The equations for Scenarios 1 and 2 differ only in that for Scenario 1 the rate constants k_{1cat} and k_{2cat} are set to zero. For these scenarios, the equations for the solution phase are:

2.2.1. *Solution phase equations*

$$\frac{de_1}{dt} = -k_{1on}e_1\left\{r_1^{Tv} - e_1^{mv} - z_1^{mv}\right\} + k_{1off}e_1^{mv} + \frac{k_{1cat}e_2z_1}{K_{1M} + z_1} - k_{1in}e_1 \quad (13)$$

$$\frac{dz_1}{dt} = -k_{1on}^z z_1\left\{r_1^{Tv} - e_1^{mv} - z_1^{mv}\right\} + k_{1off}^z z_1^{mv} - \frac{k_{1cat}e_2z_1}{K_{1M} + z_1} \quad (14)$$

$$\frac{de_2}{dt} = -k_{2on}e_2\left\{r_2^{Tv} - e_2^{mv} - z_2^{mv}\right\} + k_{2off}e_2^{mv} + \frac{k_{2cat}e_1z_2}{K_{2M} + z_2} - k_{2in}e_2 \quad (15)$$

$$\frac{dz_2}{dt} = -k_{2on}^z z_2\left\{r_2^{Tv} - e_2^{mv} - z_2^{mv}\right\} + k_{2off}^z z_2^{mv} - \frac{k_{2cat}e_1z_2}{K_{2M+z_2}} \quad (16)$$

The equations for the membrane phase are:

2.2.2. *Membrane phase equations*

$$\frac{de_1^{mv}}{dt} = k_{1on}e_1\left\{r_1^{Tv} - e_1^{mv} - z_1^{mv}\right\} - k_{1off}e_1^{mv} + \frac{k_{1cat}^m e_2^{mv} z_1^{mv}}{K_{1M}^{mv} + z_1^{mv}} - k_{1in}^m e_1^{mv} \quad (17)$$

$$\frac{dz_1^{mv}}{dt} = k_{1on}^z z_1\left\{r_1^{Tv} - e_1^{mv} - z_1^{mv}\right\} - k_{1off}^z z_1^{mv} - \frac{k_{1cat}^m e_2^{mv} z_1^{mv}}{K_{1M}^{mv} + z_1^{mv}} \quad (18)$$

$$\frac{de_2^{mv}}{dt} = k_{2on}e_2\left\{r_2^{Tv} - e_2^{mv} - z_2^{mv}\right\} - k_{2off}e_2^{mv} + \frac{k_{2cat}^m e_1^{mv} z_2^{mv}}{K_{2M}^{mv} + z_2^{mv}} - k_{2in}^m e_2^{mv} \quad (19)$$

$$\frac{dz_2^{mv}}{dt} = k_{2on}^z z_2\left\{r_2^{Tv} - e_2^{mv} - z_2^{mv}\right\} - k_{2off}^z z_2^{mv} - \frac{k_{2cat}^m e_2^{mv} z_2^{mv}}{K_{2M}^{mv} + z_2^{mv}} \quad (20)$$

The results we present in the next section were obtained by linearized stability analysis (Edelstein-Keshet, 1988) of eqns (13–20) and numerical solution of eqns (1–12) or eqns (13–20). For the numerical solution of the equations, we handle the solution-phase and membrane-phase kinetic terms with methods for stiff ordinary differential equations implemented in the software package LSODE (Hindmarsh, 1983), and we solve the diffusion terms using the Crank–Nicolson method (Morton & Mayers, 1994). Because we are particularly interested in resolving events near the membrane, we use a spatial grid over $[0, y_{max}]$ that has a uniform fine space step over the interval $[0, 0.2*y_{max}]$, a uniform coarse space step over $[0.5*y_{max}, y_{max}]$, and a variable space step that increases gradually from the fine to the coarse size step over the remaining middle portion of the domain. We have done careful numerical convergence tests to ensure the validity of our numerical solutions.

3. Results

In this section we present the results of a linearized stability analysis of the equations for Scenarios 1

and 2; computational solution of the full nonlinear equations for these Scenarios; and computational solution of the equations for Scenario 3 with finite-rate diffusion.

3.1. RESULTS OF LINEARIZED STABILITY ANALYSIS

The only nonzero steady-state solution of eqns (13)–(20) has no enzyme either in solution or bound to the membrane, and has zymogen concentrations z_1^*, $(z_1^{mv})^*$, z_2^*, and $(z_2^{mv})^*$ which are related by the equilibrium conditions,

$$(z_1^{mv})^* = \frac{z_1^*}{K_{1D}^z + z_1^*} r_1^{Tv} \text{ and } (z_2^{mv})^* = \frac{z_2^*}{K_{2D}^z + z_2^*} r_2^{Tv} \quad (21)$$

where $K_{1D}^z = k_{1off}^z/k_{1on}^z$ and $K_{2D}^z = k_{2off}^z/k_{2on}^z$. We imagine that this steady state is perturbed slightly by the addition of trace amounts of enzyme, and we ask whether this perturbation grows in time or decays away.

While these perturbations are small, their dynamics are well described by the linear system of equations obtained by linearizing eqns (13)–(20) about the steady-state solution. The linearized equations can be written in matrix form as:

$$\frac{\mathrm{d}\mathbf{e}}{\mathrm{d}t} = \mathbf{A}\mathbf{e} \quad (22)$$

where $\mathbf{e}$ is the vector with components e_1, e_1^{mv}, e_2, and e_2^{mv}, and $\mathbf{A}$ is a 4-by-4 matrix given in the Appendix. The perturbations decay and the system is called *linearly stable* if all of the eigenvalues of $\mathbf{A}$ have negative real part. The perturbations grow exponentially and the system is deemed *linearly unstable* if one or more of these eigenvalues has positive real part. By using the Routh–Hurwitz condition (see the Appendix), we have established that for Scenario 1, in which there is no solution-phase enzyme activation, the system is (linearly) stable if and only if

$$\left[\frac{k_{1cat}^m\left(\frac{z_1^*}{K_{1D}^z + z_1^*}\right)r_1^{Tv}}{K_{1M}^{mv} + \left(\frac{z_1^*}{K_{1D}^z + z_1^*}\right)r_1^{Tv}}\right]\left[\frac{k_{2cat}^m\left(\frac{z_2^*}{K_{2D}^z + z_2^*}\right)r_2^{Tv}}{K_{2M}^{mv} + \left(\frac{z_2^*}{K_{2D}^z + z_2^*}\right)r_2^{Tv}}\right]$$
$$\left[k_{1in}^m + \frac{k_{1in}k_{1off}}{k_{1on}\left(1 - \frac{z_1^*}{K_{1D}^z + z_1^*}\right)r_1^{Tv} + k_{1in}}\right]$$
$$\times \left[k_{2in}^m + \frac{k_{2in}k_{2off}}{k_{2on}\left(1 - \frac{z_2^*}{K_{2D}^z + z_2^*}\right)r_2^{Tv} + k_{2in}}\right]. \quad (23)$$

This threshold condition is similar to that found by Beltrami & Jesty (Jesty *et al*., 1993) for solution phase enzyme interactions but with one important difference. The Beltrami–Jesty condition does *not* include the surface binding-site densities r_1^{Tv} and r_2^{Tv}. To see the importance of this difference, first suppose that

$$k_{1in} \gg k_{1on}\left(1 - \frac{z_1^*}{K_{1D}^z + z_1^*}\right)r_1^{Tv}$$

and

$$k_{2in} \gg k_{2on}\left(1 - \frac{z_2^*}{K_{2D}^z + z_2^*}\right)r_2^{Tv}. \quad (24)$$

Then, the right-side of the inequality in (23) reduces approximately to $(k_{1in}^m + k_{1off})(k_{2in}^m + k_{2off})$. With this reduction, the inequality says the system is stable provided the product of the rates of removal of the enzymes from the membrane exceeds the product of the rates of activation of the enzymes. This is essentially the condition that Beltrami and Jesty found. Suppose that (24) hold, and that the other parameter values are such that (23) is satisfied. Now suppose that the concentrations of the binding sites, r_1^{Tv} and r_2^{Tv} are increased. The left-side of (23) is an increasing function of r_1^{Tv} and r_2^{Tv}, and the denominators of the terms on the right-side in (23) are increasing functions of r_1^{Tv} and r_2^{Tv}. Hence, the increase in r_1^{Tv} and r_2^{Tv} causes the left-side to increase and the right-side to decrease and thus makes it easier for the inequality to be violated and for the system to become unstable. Thus, changes in the binding-site densities can modulate the threshold condition, and in the absence of any other changes, push a stable system over the threshold for instability. We consider this further below.

For Scenario 2, in which enzyme activation can take place both on the membrane surface and in solution, the linearized stability analysis is a little more complicated. The reason for this is that enough enzymatic activity in either the solution phase or the membrane phase can destabilize the system. The precise stability conditions for Scenario 2 are given in the Appendix.

In Fig. 3, we plot regions of linear stability in the (r_1^{Tv}, r_2^{Tv})-plane for various physically-plausible choices of the kinetic parameters. The parameter values which give rise to Fig. 3(a) and 3(b) differ only in that the inhibition rates k_{1in}, k_{2in}, k_{1in}^m, and k_{2in}^m are a factor of 3 larger in 3(b). These plots are symmetric in r_1^{Tv} and r_2^{Tv} because the kinetic parameters were set symmetrically, e.g. $k_{1in} = k_{2in}$, $k_{1on} = k_{2on}$, and so on. When k_{1cat} and k_{2cat} are increased from zero to non-zero values, the region of stability shrinks as shown in Fig. 3(c).

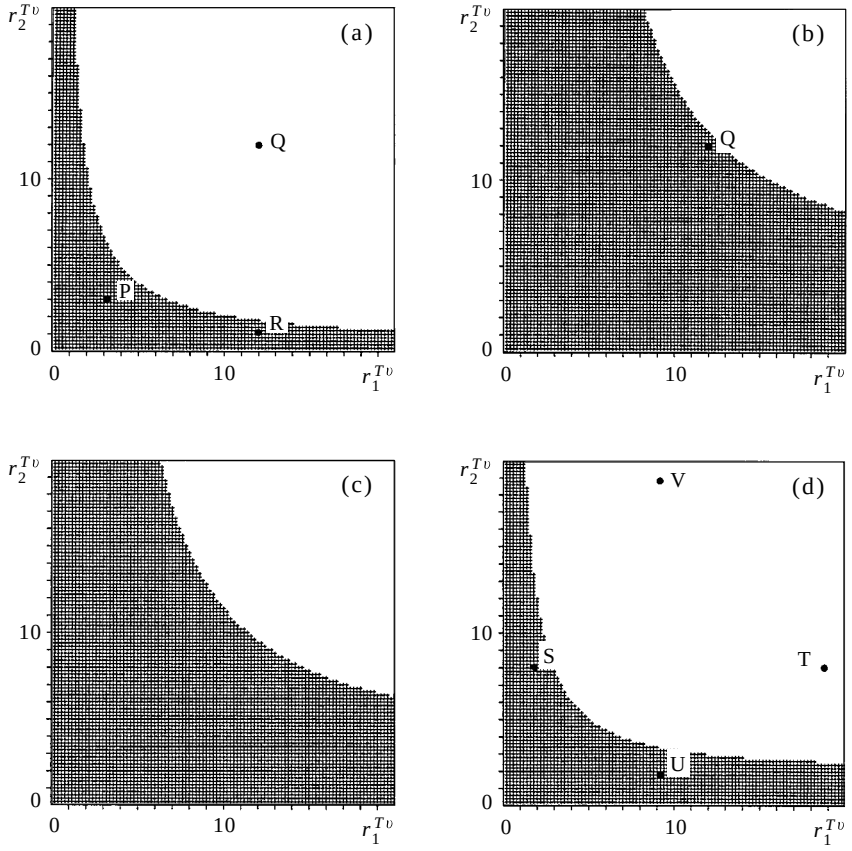

FIG. 3. Stable (shaded) and unstable regions in (r_1^{Tv}, r_2^{Tv}) plane: (a) $k_{1on} = k_{2on} = k_{1on}^z = k_{2on}^z = 0.01$, $k_{1off} = k_{2off} = k_{1off}^z = k_{2off}^z = 0.1$, $k_{1cat}^m = k_{2cat}^m = 1.0$, $K_{1M}^{mv} = K_{2M}^{mv} = 10.0$, $k_{1cat} = k_{2cat} = 0$. $K_{1M} = K_{2M} = 10.0$, $k_{1in} = k_{2in} = k_{1in}^m = k_{2in}^m = 0.1$. $z_1^* = z_2^* = 10.0$; (b) same as (a) except $k_{1in} = k_{2in} = k_{1in}^m = k_{2in}^m = 0.3$; (c) same as (b) except $k_{1cat} = k_{2cat} = 0.5$; (d) same as (a) except $k_{2cat}^m = 0$ and $k_{2cat} = 2.0$. Volume concentrations measured in nM, first order rates in s^{-1}, second-order rates in nM s^{-1}, and time in s.

When the kinetic parameters for (E_1, Z_1) differ from those for (E_2, Z_2), the stability regions may become asymmetrical to reflect this, as in Fig. 3(d).

3.2. COMPUTATIONAL SOLUTIONS FOR SCENARIOS 1 AND 2:

In Fig. 4 we show the difference in how the system behaves when it is below or above threshold and is

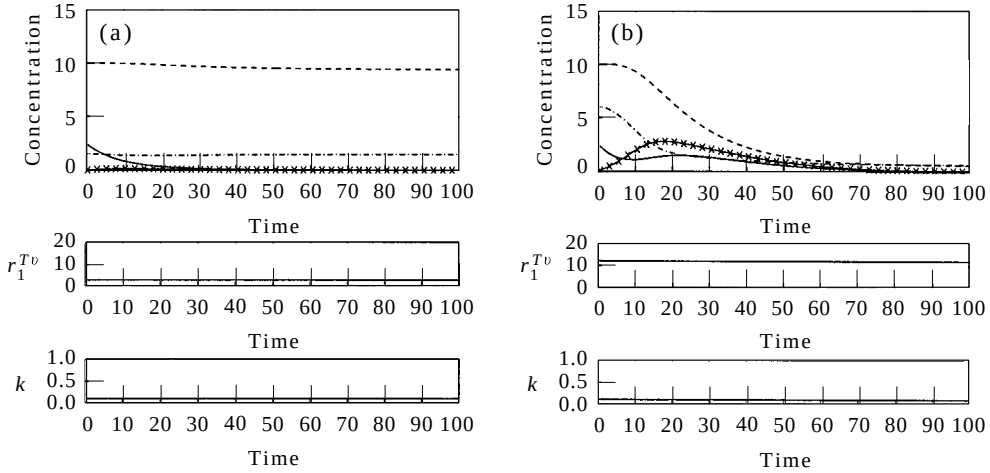

FIG. 4. Time course of reaction dynamics: top panels show $e_1 = e_2$ (—), $e_1^{mv} = e_2^{mv}$ (—x—), $z_1 = z_2$ (– – –), and $z_1^{mv} = z_2^{mv}$ (–·–·–) vs. t. Middle panels shows $r_1^{Tv} = r_2^{Tv}$ vs. t and bottom panels show $k_{1in} = k_{1in}^m = k_{2in} = k_{2in}^m$ vs. t. The parameter values at $t = 0$ for the left and right panels correspond, respectively, to the stable point P and to the unstable point Q in Fig. 3(a).

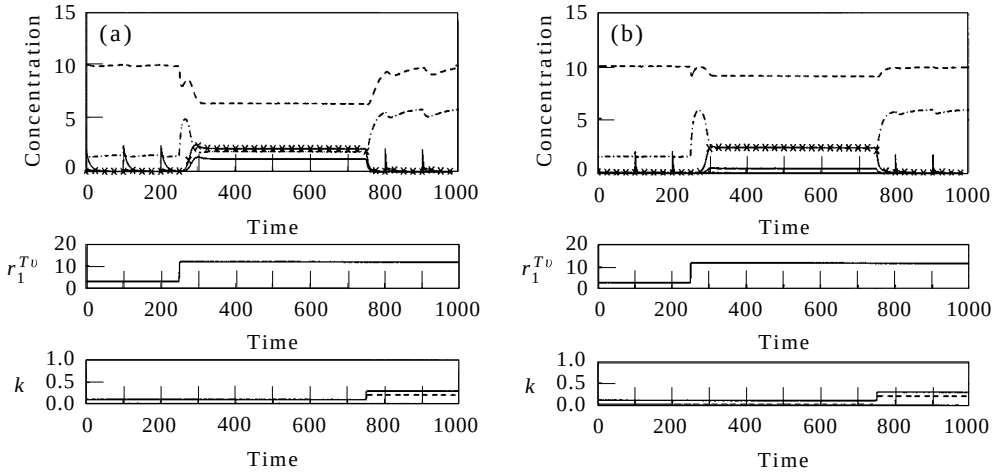

FIG. 5. Time course of reaction dynamics: enzymes activated only on membrane: (a) top panel shows e_1 (—), e_1^{mv} (—x—), z_1 (– – –), and z_1^{mv} (–·–·–) vs. t. Middle panel shows r_1^{Tv} vs. t and bottom panel shows $k_{1in} = k_{1in}^m$ vs. t. Parameter values at $t = 0$ are as in Fig. 3(a) except $k_{1in} = k_{2in} = 0.01$ and $f = 0.09$; (b) same as (a) except $f = 0.49$.

stimulated by the addition of a small increment of enzyme. In Fig. 4(a), we see that if the below-threshold system is stimulated, the enzyme decays quickly and monotonically to 0. In Fig. 4(b) we see that when the above-threshold system is stimulated, enzyme levels rise substantially and fall only as the zymogen in the system is consumed.

In Figs 5–7, we show results from computational solution of the nonlinear equations (13–20) with the "flow" terms $-fe_1$, $f(z_1^{up} - z_1)$, $-fe_2$, and $f(z_2^{up} - z_2)$ added to the right-sides of (13–16), respectively, to allow replenishment of solution-phase zymogen and removal of solution-phase enzyme. Here f is a rate constant which specifies how rapidly zymogens Z_1 and Z_2 are added to the system at their "upstream" concentrations z_1^{up} and z_2^{up}, respectively, and how rapidly these zymogens and enzymes E_1 and E_2 are removed from the system by the flow. At steady state, the flow terms set the solution-phase zymogen concentrations to their "upstream" values z_1^{up} and z_2^{up}. The steady-state membrane-phase zymogen densities are still related to these by (21). The linear stability analysis of the modified system is almost the same as for the original system (13–20). The only difference is that each occurrence of k_{1in} and k_{2in} in (23–28) is replaced by $k_{1in} + f$ and $k_{2in} + f$, respectively. Thus, in the linear analysis, the effect of flow is stabilizing because it carries away solution-phase enzyme. In the full nonlinear system, the flow also replenishes zymogen whenever the solution-phase zymogen

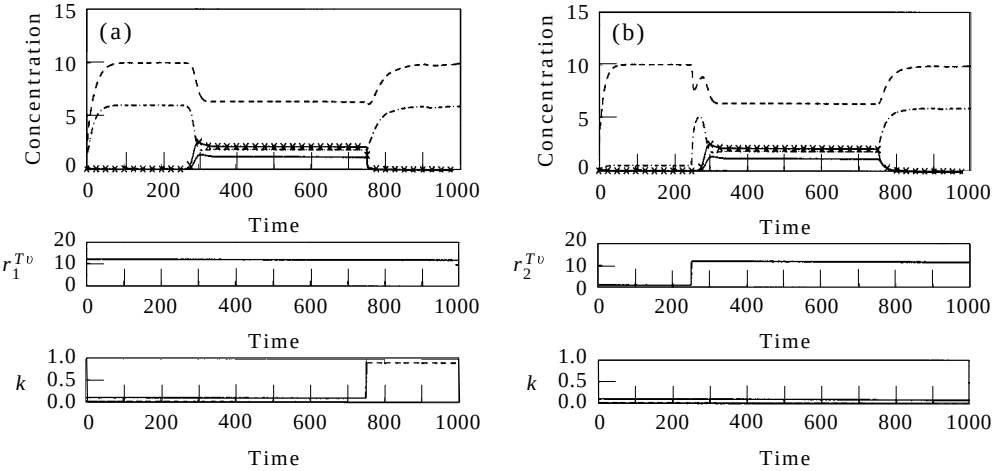

FIG. 6. Time course of reaction dynamics: enzymes activated only on membrane: (a) top panel shows e_1 (—), e_1^{mv} (—x—), z_1 (– – –), and z_1^{mv} (–·–·–) vs. t. Middle panels shows r_1^{Tv} vs. t and bottom panel shows $k_{1in} = k_{1in}^m$ vs. t; (b) top panel shows e_2 (—), e_2^{mv} (—x—), z_2 (– – –), and z_2^{mv} (–·–·–) vs. t. Middle panel shows r_2^{Tv} vs. t and bottom panel shows $k_{2in} = k_{2in}^m$ vs. t. Parameter values at $t = 0$ are as in Fig. 5(a).

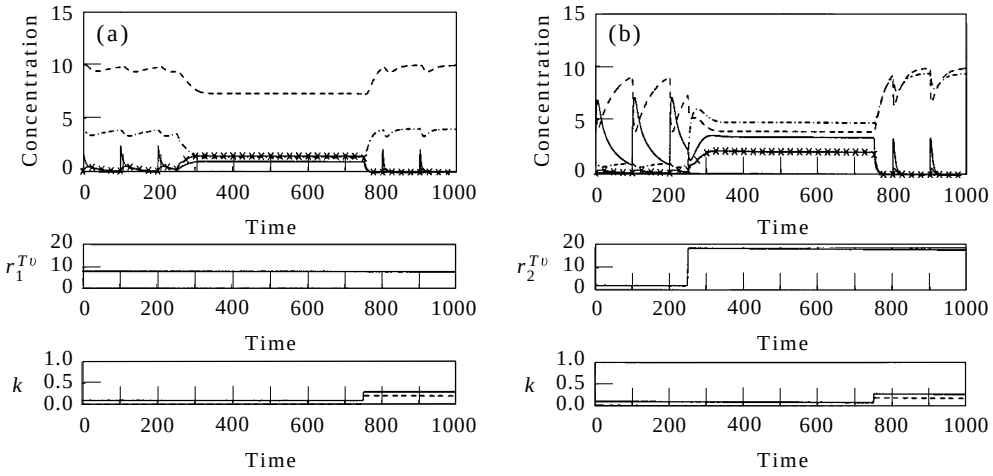

FIG. 7. Time course of reaction dynamics: enzyme E_1 activated only on membrane; enzyme E_2 activated only in solution: (a) top panel shows e_1 (—), e_1^{mv} (—x—), z_1 (– – –), and z_1^{mv} (–·–·–) vs. t. Middle panels shows r_1^{Tv} vs. t and bottom panel shows $k_{1in} = k_{1in}^m$ vs. t; (b) top panel shows e_2 (—), e_2^{mv} (—x—), z_2 (– – –), and z_2^{mv} (–·–·–) vs. t. Middle panel shows r_2^{Tv} vs. t and bottom panel shows $k_{2in} = k_{2in}^m$ vs. t. Parameter values at $t = 0$ are as in Fig. 3(d) except $k_{1in} = k_{2in} = 0.01$ and $f = 0.09$.

concentrations in the system fall below the specified "upstream" values. For all of the following experiments we set $z_1^{up} = z_2^{up} = 10.0$.

In Fig. 5(a), we show results from a computational experiment in which the kinetic parameters were set to the values used to generate Fig. 3(a) except that k_{1in} and k_{2in} were set to 0.01 and the flow rate was set to $f = 0.09$. As noted above, the effect of flow on linearized stability is found by replacing k_{1in} and k_{2in} in (23–28) by $k_{1in} + f$ and $k_{2in} + f$, respectively. The choices of k_{1in}, k_{2in}, and f here thus correspond to the parameters of Fig. 3(a). The surface binding-site densities were held at $r_1^{Tv} = r_2^{Tv} = 3.0$ until time $t = 250$. This corresponds to point P in Fig. 3(a) which is in the stable region. The system behaved stably despite our addition of small increments to the solution-phase enzyme concentrations at times $t = 0$, $t = 100$ and $t = 200$. Indeed, we see that these perturbations decayed quickly. At time $t = 250$, we increased r_1^{Tv} and r_2^{Tv} quickly, but continuously, to $r_1^{Tv} = r_2^{Tv} = 12.0$ which corresponds to point Q in Fig. 3(a). This point is in the unstable region, and this is reflected in the observed dynamics. The membrane-bound zymogen concentration rose quickly following our increase in r_1^{Tv} and r_2^{Tv}. After a short lag period, the membrane-bound and solution-phase enzyme concentrations rose rapidly and plateaued at new high levels, while the membrane-bound zymogen concentration dropped. The stimulus for the rapid rise in enzyme levels was the residual enzyme remaining from the last exogenous increment given at $t = 200$ as we gave no further increments while the stability inequality (23) was violated. The system remained in its new state until time $t = 750$ when we increased the inhibition rates k_{1in}, k_{2in}, k_{1in}^m, and k_{2in}^m by 0.2. This change in kinetic parameters changed the stable region in the (r_1^{Tv}, r_1^{Tv}) plane to that shown in Fig. 3(b). The point Q still represents the binding-site densities in our system, but this point is now in the stable region. As shown in Fig. 5(a), the enzyme levels rapidly plummeted to values near 0, and the bound zymogen levels increased to their equilibrium levels [see eqn (21)] for the high binding-site densities. This computational experiment makes explicit the potential of variations in surface-binding densities and inhibition parameters to serve as a biological "switch" to turn-on or turn-off rapid enzyme production in this system. In Fig. 5(b), we perform an identical experiment except that the flow rate was set to $f = 0.49$. The increased flow rate had several effects: The lag period between the increase in binding-site density and the sharp rise in enzyme concentrations lengthened significantly. The solution-phase zymogen levels were held closer to their "upstream" values. The solution-phase enzyme levels decreased. When experiments were run that were identical to those depicted in Fig. 5 except that the solution-phase enzymatic rate constants k_{1cat} and k_{2cat} were set to 1 rather than 0, the only difference in the results was that the enzyme concentrations reached higher plateaus during the system's "on" state.

For the experiments of Fig. 5, increases in *both* r_1^{Tv} and r_2^{Tv} were used to trigger the start of substantial enzymatic activity, and increases in *all* four of the inhibition rates, k_{1in}, k_{1in}^m, k_{2in}, and k_{2in}^m were used to turn off this activity. That this is more than is necessary is shown by the experiment depicted in Fig. 6. For this experiment, r_1^{Tv} was held at a high level

from the outset, and r_2^{Tv} started at a low level. The point R in Fig. 3(a) shows the initial values of (r_1^{Tv}, r_2^{Tv}) and is in the stable region. At time $t = 250$, r_2^{Tv} was increased to bring (r_1^{Tv}, r_2^{Tv}) to point Q in Fig. 3(a) and this change alone served to switch on enzymatic activity. Similarly, inhibition rates k_{2in} and k_{2in}^m were kept at low levels throughout the calculation, and only the increase of k_{1in} and k_{1in}^m caused the enzymatic activity to be turned off. The values of k_{1in} and k_{1in}^m required to turn the system off were greater than when all four inhibition rates were increased. This experiment shows that even with one binding-site species in excess, a paucity of the other can keep the system in its "off" state, and that similarly, sufficiently large increases in the inhibition of just one of the enzyme reactions can turn off the entire system.

Figure 7 shows an experiment in which enzyme E_1 could be activated only on the surface, while E_2 could be activated only in solution. All of the kinetic and flow parameters are the same as for the experiment of Fig. 5(a) except here $k_{2cat}^m = 0$ and $k_{2cat} = 2.0$. The stable and unstable binding densities for these kinetic parameters are shown in Fig. 3(d). Values of the surface binding densities at $t = 0$ correspond to point U in the stable region. The system was challenged with small increments of solution-phase e_1 and e_2 at times $t = 0$, 100, and 200. We see that in response to each stimulus, e_2 increased rapidly to high peaks but also rapidly decayed away so there was no sustained increase in e_2 levels. At $t = 250$, the binding site density r_2^{Tv} was increased from 2.0 to 19.0 [corresponding to point V in the unstable region of Fig. 3(d)] and the system responded with large and sustained increases in both e_2 and e_2^{mv} and with smaller but sustained increases in e_1 and e_1^{mv}. These new enzyme levels persisted until the inhibition rates were increased at $t = 750$ after which time they dropped to 0. For this experiment, the increase of r_2^{Tv} allowed solution-phase E_2 to bind to the membrane where it could activate membrane-bound Z_1 to E_1. Some of the membrane-bound E_1 dissociated and was able to activate solution-phase Z_2 to E_2 at a rate that balanced the decay of E_2. Similar behavior was seen when the binding-site densities (r_1^{Tv}, r_2^{Tv}) began at point S of Fig. 3(d) and were changed by increasing r_1^{Tv} to point T. So a variation of the system in which one enzyme is activated on the membrane and the other in solution still displays threshold responses that can be modulated by changing either of the binding-site densities. One interesting difference between the behavior of this variation compared to that when both enzymes were activated on the membrane was seen when the flow rate was increased from $f = 0.09$ to $f = 0.49$. In contrast to the results shown in Fig. 5(b), here the system *never* was excited to sustained higher enzyme levels. Apparently the flow removed the solution-phase enzymes too quickly for this to occur. It is also interesting that even with $f = 0.09$, we had to set k_{2cat}/K_{2M} higher than k_{2cat}^m/K_{2M}^m in Fig. 5 in order to achieve comparable levels of enzyme activation.

3.3. COMPUTATIONAL SOLUTIONS FOR SCENARIO 3

We now turn to Scenario 3 and eqns (1–12) which allow for differences in concentration at different spatial points, and which take into account diffusion within the solution-phase, and between the solution phase and the membrane phase. Our main concern in discussing these equations in this paper is to what extent the threshold conditions just derived persist in the presence of finite-rate diffusion, and therefore whether variations in binding-site densities and inhibition rates can serve, respectively, to turn on and turn off enzyme production as they can in the spatially homogeneous cases above.

There are two distinct physical situations that are interesting to consider and which suggest two different variations on how the diffusion problem should be set up. The first situation corresponds to the *in vivo* setting in which the membrane surface of interest is that of the vessel wall or of wall-adherent platelets, and the bulk solution flows over this surface. In this case, variations in surface binding-site density arise because of different degrees of expression of these receptors on the surface at different times. The amount of surface stays the same but the density of binding sites on the surface changes. The second situation corresponds to experiments that have been done with artificial phospholipid vesicles (Krishnaswamy *et al*., 1993, Ye & Esmon, 1995). Here, both the surface density of binding sites on a vesicle and the volume concentration of vesicles can be manipulated to change the volume concentration of binding sites. In the first *in vivo* setting, one can imagine that the bulk flow passing over the membrane serves to keep approximately constant the concentration of solution-phase zymogen and enzyme at a fixed distance from the surface. This suggests that fixing these concentrations at a location $y = y_{max}$ is reasonable. Furthermore, in this setting, variations in binding-site density are introduced by explicit variations in r_1^T and r_2^T. For the second setting, one can imagine that the vesicles and solution-phase chemicals are well-mixed in the sense that what happens in a volume around any particular vesicle is the same as what happens in an equal volume around any other vesicle. This would not be a reasonable assumption if the vesicles were

present in very high concentration. For then, the ratio of the concentration of vesicles to that of enzyme or zymogen would be so high that in the volume around each vesicle there would be at most a few molecules of zymogen or enzyme. But we are interested in situations in which the concentration of binding-sites is small enough to be the controlling variable, and then this picture of a representative vesicle and surrounding volume seems reasonable. For this case, we solve the equations in the domain $y_{min} \leqslant y \leqslant y_{min} + y_{max}$ where y_{min} is the *radius* of the vesicle. The symmetries in the problem imply that there is no net flux of solution-phase zymogen or enzyme across the boundary $y = y_{min} + y_{max}$ of the representative volume, and so the boundary conditions imposed at $y = y_{min} + y_{max}$ are $\partial z_1/\partial y = \partial e_1/\partial y = \partial z_2/\partial y = \partial e_2/\partial y = 0$. For this type of simulation we replaced the diffusion operator $\partial^2/\partial y^2$ in Cartesian coordinates with $\partial^2/\partial y^2 + 2/y\,\partial/\partial y$ because here we view y as the radial variable in spherical coordinates. There are now two ways that the volume concentration of binding sites can be varied: one is by varying the surface density (r_1^T) of membrane-binding sites to reflect changes in vesicle constituents; the second is by varying the concentration of vesicles. This latter is carried out by varying the thickness y_{max} of the solution phase region within a representative volume; a decrease in y_{max} corresponds to an increase in vesicle concentration. For vesicles of radius 50 nm, $y_{max} = 1.0\ \mu$m corresponds to a vesicle volume concentration of approximately 0.3 nM.

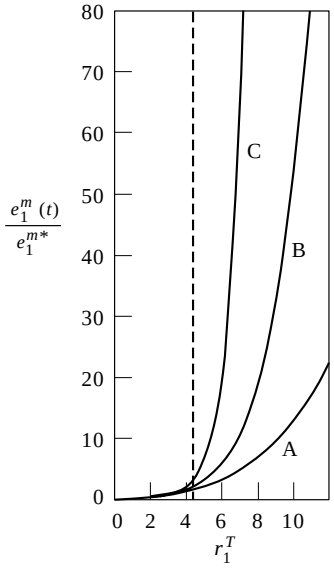

FIG. 8. Effects of diffusive transport: membrane-bound enzyme density vs. r_1^T at times: (A) 10 s, (B) 20 s, (C) 50 s. Curves at later times were virtually identical to the 50 s curve. (– – –) indicates threshold value of r_1^T for spatially-homogeneous system. Kinetic parameters are as in Fig. 3(a), and $D_1 = D_2 = 5.(10)^{-7}\,\text{cm}^2\,\text{s}^{-1}$. Binding-site densities are measured in $10^{-14}\,\text{M}/100\,\text{cm}^2$, time in s, and enzyme densities are relative to e_1^{m*}, the density at $t = 0$ with $r_1^T = 4.4$.

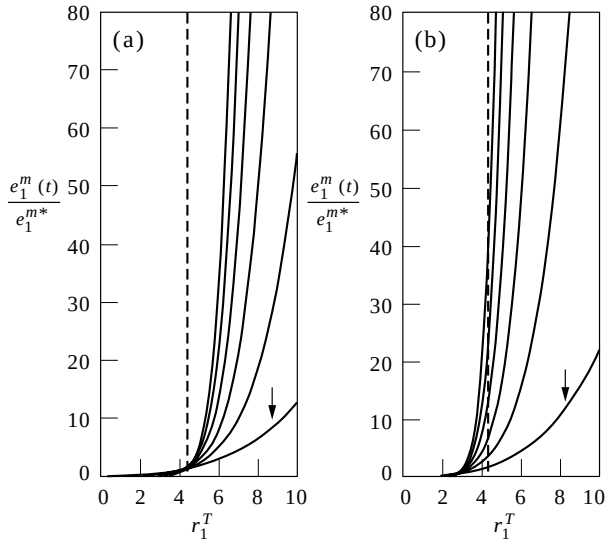

FIG. 9. Effects of diffusive transport: membrane-bound enzyme density vs. r_1^T at selected times with (a) $y_{max} = 1.0\ \mu$m and (b) $y_{max} = 10.0\ \mu$m. Arrow shows curve for $t = 10$ s; curves for $t = 20$, 30, 40 s, ... rise progressively more steeply. Binding site densities are in relative units (see text), and enzyme densities are relative to e_1^{m*}, the density at $t = 0$ with $r_1^T = 4.4$. (– – –) indicates threshold values of r_1^T for spatially-homogeneous system. Kinetic parameters are as in Fig. 3(a), and $D_1 = D_2 = 5.(10)^{-7}\,\text{cm}^2/\text{s}$. Vesicle radius = 50 nm.

In Fig. 8, we show results from simulations of the first kind in which the concentrations of zymogens and enzymes were held fixed at a distance of 1.0 μm from the membrane, and we looked at how the production of enzyme changed as the surface density of binding sites was varied. The experiments shown were done with symmetric choices of kinetic parameters and initial enzyme and zymogen concentrations, and therefore $e_1^m(t) = e_2^m(t)$, $e_1(y, t) = e_2(y, t)$, etc. at each location y and time t. It is evident from Fig. 8 that the system with finite-rate diffusion still displays threshold-like behavior with a threshold at approximately the same binding-site density as the spatially homogeneous system. As a consequence, variations in binding-site densities and inhibition rates can indeed serve as switches for enzyme production even with finite-rate diffusion (results not shown).

Figures 9–10 show results from experiments of the second kind in which no-flux conditions were imposed on the concentrations of zymogen and enzyme at $y = y_{min} + y_{max}$. As in Fig. 8, these experiments were done with symmetric choices of kinetic parameters and initial enzyme and zymogen concentrations. In the first set of these experiments, the binding-site densities $r_1^T = r_2^T$ were varied for each of several values

of the thickness y_{max} of the solution phase region within the representative volume. The calculations shown were done for vesicles of radius 50 nm. Each frame in Fig. 9 corresponds to a different y_{max} as r_1^T was varied. As we can see, threshold behavior like that of the spatially-homogeneous system is again displayed. To see whether diffusion and vesicle concentration alters the actual threshold level from that predicted for the spatially-homogeneous case of Scenario 1, we proceeded as follows: the volume concentration of binding sites here is the same as r_1^{Tv} of Scenario 1 if the surface density r_1^T is related to r_1^{Tv} by $r_1^{Tv} = \gamma r_1^{Tv}$, where

$$\gamma = \left[\frac{4\pi y_{min}^2}{(4\pi/3)(y_{min} + y_{max})^3} \right]$$

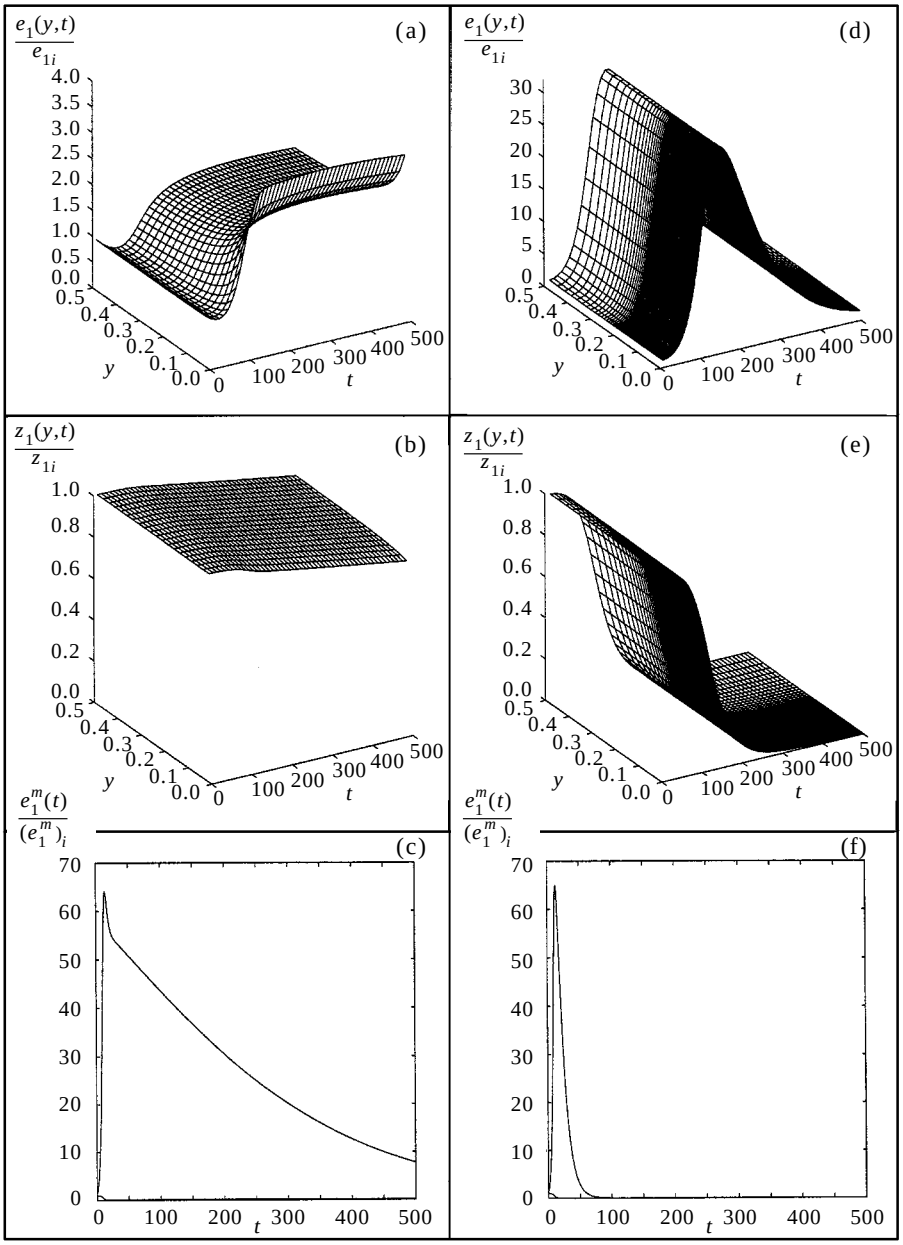

FIG. 10. Relative $e_1(y_{min} + y, t)$ and $z_1(y_{min} + y, t)$ vs. y and t and relative $e_1^m(t)$ vs. t for vesicles of radius $y_{min} = 50$ nm and various y_{max}. e_{1i}, z_{1i} are initial solution-phase enzyme and zymogen concentrations, and $(e_1^m)_i$ is initial membrane-bound enzyme density: (a) e_1; (b) z_1; and (c) e_1^m for $y_{max} = 5.0$ μm; (d) e_1; (e) z_1; and (f) e_1^m for $y_{max} = 1.0$ μm. Kinetic parameters are as in Fig. 3(a), $D_1 = D_2 = 5.(10)^{-7}$ cm^2 s^{-1}, and $r_1^T = 0.46(10)^{-10}$ moles/(100 cm^2).

TABLE 2
Relation between y_{max} *and predicted threshold value of* r_1^T

y_{max} (μm)	$r_{1\,\text{threshold}}^T$ (moles/100 cm^2)
10.0	$0.596\,(10)^{-8}$
5.0	$0.756\,(10)^{-9}$
1.0	$0.679\,(10)^{-11}$
0.1	$0.198\,(10)^{-13}$

Threshold values of binding-site surface density as predicted by the spatially-homogeneous system for vesicles of radius $y_{min} = 50$ nm, and for various thicknesses y_{max} of the representative volume.

In particular, since the threshold level in Scenario 1 (for our choice of kinetic parameters) is $r_1^{Tv} = 4.4$ nM, the corresponding predicted threshold levels here would be 4.4 nM divided by γ. In Fig. 9, r_1^T is plotted in units of 1.0 nM divided by γ, and so, in these plots, the predicted threshold level is always 4.4. The actual surface density to which this value corresponds varies with y_{min} and y_{max}; the actual values for $y_{min} = 50$ nm, and for the y_{max} studied are given in Table 2. We note that the volume membrane-phase K_{1M}^{mv} from Scenario 1 and the surface membrane-phase K_{1M}^{m} here are also related by $K_{1M}^{mv} = \gamma K_{1M}^{m}$. Figure 9 shows that the observed threshold level is in quite good agreement with the spatially-homogeneous case for $y_{max} = 1.0\ \mu$m, and occurs at lower values of the scaled r_1^T than for the homogeneous case when $y_{max} = 10.0\ \mu$m. (Not shown is the fact that the threshold level is in good agreement with the spatially-homogeneous case for $y_{max} = 0.1\ \mu$m as well.) Because of the way the scaling is done, the actual density of surface binding sites at a particular r_1^T in the figure is much higher for $y_{max} = 10.0\ \mu$m than for the smaller y_{max}, and it seems that these very high surface densities make the system respond more strongly than the homogeneous situation would suggest. An alternative way to think of this is that when the vesicle concentration is high (small y_{max}), the homogeneous system is a good predictor; but when the vesicles are widely separated (large y_{max}), and the surface densities are high, the system is too inhomogeneous spatially for the homogeneous system to make good predictions about its behavior.

Figure 10 shows the effect of y_{max} on the solution-phase enzyme and zymogen concentrations. Here, the surface density of binding sites was held fixed as y_{max} was varied. The two columns of panels are for vesicles of radius $y_{min} = 50$ nm, and $y_{max} = 5.0\ \mu$m and $1.0\ \mu$m, respectively. In each case, we show $e_1(y_{min} + y, t)$ and $z_1(y_{min} + y, t)$ only for $0 \leqslant y \leqslant 0.50\ \mu$m. We also show $e_1^m(t)$ vs. t. The membrane enzyme density peaks at approximately the same value and at approximately the same time in both cases. Even so, the spatial distribution of solution-phase enzyme and zymogen is very different when $y_{max} = 5.0\ \mu$m compared with $y_{max} = 1.0\ \mu$m. These differences strongly influence the time evolution of the membrane enzyme densities after the peak. For $y_{max} = 1.00\ \mu$m, diffusion quickly leads to near equilibration of e_1 and z_1 over the solution phase. Because there is little spatial gradient in z_1, there is little diffusive flux of zymogen to the surface, and thus little new production of enzyme. The enzyme concentration decays almost uniformly in y due to inactivation. For $y_{max} = 5.0\ \mu$m, diffusion does not completely equilibrate the solution-phase concentrations during the time period shown. The zymogen concentration continues to show a significant gradient as one moves away from the surface, and the resulting diffusive flux to the surface fuels continued enzyme production. The enzyme concentration also shows a gradient, and so enzyme which dissociates from the surface can diffuse away. The net result of these processes is a much slower decay in the near surface enzyme-concentration than in the $y_{max} = 1.0\ \mu$m case.

4. Discussion

We have formulated and analysed the differential equations which govern the kinetics of a model two-zymogen, two-enzyme system with surface binding to learn how variations in surface binding-site density and inactivation rates can team to regulate the production of enzyme. These studies involve a positive feedback loop, in which increased concentration (or surface density) of each enzyme can, under certain conditions, stimulate increased production of the other enzyme. Our main conclusions are that the system responds in a threshold manner; that an increase in the availability of surface binding sites can *switch* the state of the system from one in which stimuli decay quickly away, to one in which substantial and sustained production of enzyme occurs; and that a subsequent increase in inactivation rates can return the system to a state in which enzyme concentrations decay away and enzyme production ceases.

We formulated and studied the model system in the hope that we would gain insight into the workings of the more complex coagulation system. The model system matches no part of the coagulation system exactly. It corresponds most closely perhaps to the feedback loop comprised of Tissue Factor exposed on the subendothelial matrix, and Factors VII, VIIa, X, and Xa, with inhibition by the complex TFPI:Xa. Here, it is the exposure of Tissue Factor which corresponds to the increase of surface binding sites in

the model. The model system also corresponds roughly to the interaction between the prothrombinase (Va:Xa) complex and thrombin, if one thinks of the pair Factor Va and Factor Xa as an enzyme whose activity is potentiated when thrombin activates Factor V to Factor Va, and realized when Factor Va and Factor Xa bind to an appropriate phospholipid surface. The surface binding sites in this case are anionic phospholipids exposed on platelet surfaces when the platelets are activated. Thrombin plays other roles in this interaction, which includes activating Factor VIII to Factor VIIIa which can lead to greater production of Factor Xa, and activating platelets which can lead to increased binding-site availability. The model corresponds (more weakly) to the interaction between thrombin and VIIIa:IXa if one ignores the intermediate position in the feedback loop played by prothrombinase.

To the extent that the model system does mimic the behavior of the coagulation system, our analysis makes predictions which are testable. For example, consider a solution which contains sufficiently high concentrations of Factor Xa, Factor V, prothrombin, inhibitors APC and ATIII, and to which are added phospholipid vesicles with controlled surface densities of appropriate binding sites. Suppose that this system were challenged with small amounts of Factor Va and thrombin. Then our analysis predicts that a sharp transition in enzyme production would be observed as the binding site density on the vesicles was increased. To our knowledge these experiments have not been done.

The existence of activation thresholds that can be adjusted by changes in binding-site densities would be of profound importance to the regulation of coagulation. Blood could circulate normally in a stable state in which the threshold condition (23) is not exceeded. In this state, activated enzyme, say Factor VIIa, could safely circulate without initiating coagulation. In fact, Morrissey (1995) presents evidence that about 1% of circulating Factor VII is normally activated. Slight disruptions of the endothelium that exposed small amounts of Tissue Factor would also not lead to coagulation; this provides a further safeguard against unnecessary coagulation responses. But once a substantial enough trauma occurred that the Tissue Factor levels caused the threshold condition to be exceeded, a very strong response would occur, primed by the interaction of the circulating Factor VIIa with the newly exposed Tissue Factor. Even then, the response would be localized to the immediate vicinity of surfaces on which the binding-site density was high. Initially these would be the subendothelial tissue on which Tissue Factor is exposed. Later the surfaces of wall-adherent activated platelets would express the binding sites to permit VIIIa:IXa and Va:Xa complex formation. It is interesting that our analysis suggests that near the edge of a thrombus which abuts healthy endothelial tissue one might well expect the coagulation reactions to *abruptly* shut down. As one moves from thrombus to endothelium, levels of inhibitors should increase: recall that APC is generated by the TM–thrombin complex on the surface of endothelial cells and that ATIII inhibitory activity is greatly enhanced when ATIII is activated by heparan sulfate proteoglycans also located on the endothelial surface (Rosenberg & Bauer, 1994). At the same time, the number of activated platelets and the extent of damaged vessel tissue drops as one moves from the core of the thrombus across its edge to the healthy tissue, and so the availability of pro-coagulant enzyme binding sites would decrease. Both these changes would push the system toward its stable state in which enzyme production ceases, and enzyme concentrations decay.

Other analyses of enzyme systems, in particular, that of Jesty *et al*. (1993) have produced threshold conditions. In that paper, the threshold condition is for a purely solution-phase system, and the threshold control variable is considered to be the total concentration of enzyme and zymogen. A threshold response is seen as this total concentration is varied from low to high levels. The physiological relevance of this control variable is doubtful as circulating zymogen levels are fairly constant, and we are aware of no mechanism for locally increasing zymogen concentrations in response to an injury. In our system, the main control variable is the density of surface binding sites, and this is known to change substantially when a vessel wall is injured or platelets are activated. It is also interesting that for our model, when the system is in the stable state, even a relatively large enzyme stimulus (equal to 25% of the zymogen concentration) decays away, while very small stimuli ($\ll 1\%$ of the zymogen concentration) trigger large enzyme production when the system is unstable.

For our model system, inequality (23) gives the condition which must be exceeded to turn on large-scale enzyme production. Anything which increases the ratios of off-rate (k_{ioff}, k^z_{ioff}) to on-rate (k_{ion}, k^z_{ion}) for enzyme or zymogen surface binding, increases the inhibition rates (k_{iin}, k^m_{iin}), increases the Michaelis–Menton constant K^{mv}_{iM}, or decreases k^m_{icat}, makes the system harder to activate because it increases the surface binding-site densities which are required to make the system unstable. Conversely, the opposite changes in each of these parameters makes

the system responsive to smaller increases in surface binding-site density. For given kinetic and binding parameters and solution-phase zymogen concentrations, there are numerous ways of switching the system from its stable to unstable states: Binding-site densities of both zymogen–enzyme pairs can increase from low to high levels. Alternatively, the binding-site density for one zymogen–enzyme pair might already be high, and the system changes state when the binding-site density for the other pair increases sufficiently. Another variation is that one enzyme, say E_1, is activated on the surface by membrane-bound E_2^m, and E_2 is activated in solution by solution-phase E_1. Both binding-site densities are still important since E_2 must be membrane-bound to activate membrane-bound E_1, and variations in one or both of the densities can again switch the system from its stable to unstable state. Each of these possibilities is illustrated above. In each of these cases, even the one with solution-phase activation of one enzyme, the requirement for surface binding sites localizes the reactions to the vicinity of the high binding-site density surface. In the system with solution-phase activation of one enzyme, it is harder to initiate and maintain the reactions because the solution-phase enzyme can be carried away by the flow. We illustrated this by adding an, admittedly crude, model of flow to our enzyme system.

The threshold response of the system to variations in surface binding-site density was shown to persist when the models included spatial inhomogeneities and finite-rate diffusion between the solution-phase and membrane surface. This was the case both for experiments intended to approximate the *in vivo* setting of blood flowing over a surface, and for experiments that correspond to suspensions of artificial phospholipid vesicles. By determining the transport of zymogens to the surface and enzymes away from it, diffusion affects the actual surface densities needed to cause substantial enzyme production, as well as the length of time the system continues to produce enzymes at a substantial rate.

For the computational experiments we performed, we had to select particular values for rate constants and concentrations. For many of these, only ballpark estimates are available in the coagulation literature. Therefore our simulation results should be viewed as illustrating the kinds of behavior possible in the enzyme system we examined, rather than as quantitative predictions about a real system. We emphasize that the threshold condition is exact for the model system; for any set of rate constants and zymogen concentrations, any change that reverses the sense of the threshold inequality, changes the qualitative behavior of the system from stable to unstable or *vice versa*.

Compared to *in vivo* coagulation, the model system analysed here is very much simplified. Perhaps the most severe simplifications concern the reduced size and complexity of the biochemical reaction network, the (almost) complete absence of any treatment of flow, and the limitation of diffusion to the direction perpendicular to the membrane surface. Our justification in making these simplifications is to arrive at a system in which one can begin to get insight into what regulates the more complex system. But of course, these insights need to be further tested and refined in more realistic models. To that end, we are working on more elaborate models which permit enzyme levels to influence the availability of surface binding sites (e.g. through activation of platelets) and inhibition rates (e.g. through transport of enzyme to endothelium and consequent increased production of inhibitors on the endothelium). Of equal importance, we are also working to incorporate into all of these models the effect of realistic multidimensional blood flow, as well as multidimensional solution-phase diffusion and surface-diffusion on the membranes. Two situations are of immediate interest to us: flow and coagulation around a small aggregate of platelets, and flow and coagulation near ruptured atherosclerotic plaques. Both of these studies will require solving the partial differential equations which govern the motion of the blood inside of a vessel whose geometry is made complex by the presence of wall-adherent platelets or plaque. These are very challenging calculations but ones we are prepared to do using computational techniques developed in the context of our ongoing studies of the dynamics of platelet aggregation (Fogelson, 1984; Fauci & Fogelson, 1993, Fogelson,1992, 1993).

The authors thank James Keener and Chung-Seon Yi for helpful suggestions. This work was supported in part by NSF Grant DMS-9307643.

REFERENCES

Bauer, K. A. & Rosenberg, R. D. (1987). The pathophysiology of the prethombotic state in humans: insights gained from studies using markers of hemostatic system activation. *Blood* **70,** 343–350.

Beltrami, E. & Jesty, J. (1995). Mathematical analysis of activation thresholds in enzyme-catalyzed positive feedbacks: application to the feedbacks of blood coagulation. *Proc. Natl. Acad. Sci. U.S.A.* **92,** 8744–8748.

Broze, G. J., Girard, T. J. & Novotny, W. F. (1990). Regulation of coagulation by multi-valent Kunitz-type inhibitor. *Biochemistry* **29,** 7539–7546.

DAVIE, E. W. & RANNOFF, O. D. (1964). Waterfall sequence for intrinsic coagulation. *Science* **145,** 1310–1312.
EATON, D., RODRIGUEZ, H. & VEHAR, G. A. (1986). Proteolytic processing of human factor VIII. Correlation of specific cleavages by thrombin, factor Xa, and activated protein C with activation and inactivation of factor VIII coagulant activity. *Biochemistry* **25,** 505–512.
EDELSTEIN-KESHET, L. (1988). *Mathematical Models in Biology*. New York: Random House.
ESMON, C. T. (1989). The roles of protein C and thrombomodulin in the regulation of blood coagulation. *J. Biol. Chem.* **264,** 4743–4746.
FAUCI, L. J. & FOGELSON, A. L. (1993). Truncated Newton methods and the modeling of complex immersed elastic structures. *Comm. Pure Appl. Math.* **46,** 787–818.
FOGELSON, A. L. (1984). A mathematical model and numerical method for studying platelet adhesion and aggregation during blood clotting. *J. Comput. Phys.* **56,** 111–134.
FOGELSON, A. L. (1992). Continuum models of platelet aggregation: formulation and mechanical properties. *SIAM JAM* **52,** 1089–1110.
FOGELSON, A. L. (1993). Continuum models of platelet aggregation: mechanical properties and chemically-induced phase transitions. In: *Fluid Dynamics in Biology* (Cheer, A. Y. & van Dam, C. P., eds), Contemporary Mathematics Series, pp. 279–294. Providence, RI: American Mathematical Society.
GEMMELL, C. H., TURITTO, V. T. & NEMERSON, Y. (1988). Flow as a regulator of the activation of factor X by tissue factor. *Blood* **72,** 1404–1408.
HEMKER, H. C. & KESSLER, H. (1991). Feedback mechanisms in coagulation. *Haemostasis* **21,** 189–196.
HINDMARSH, A. C. (1983). ODEPACK, A Systematized Collection of ODE Solvers. In *Scientific Computing* (Stepleman, R. S. *et al*., eds), Vol. 1 of IMACS Transactions on Scientific Computation, pp. 55–64. Amsterdam: North-Holland.
JESTY, J., BELTRAMI, E. & WILLEMS, G. (1993). Mathematical analysis of a proteolytic positive-feesback loop: dependence of lag time and enzyme yields on the initial conditions and kinetics parameters. *Biochemistry*, **32,** 6266–6274.
JONES, K. C. & MANN, K. G. (1994). A model for the tissue factor pathway to thrombin. II—mathematical simulation. *J. Biol. Chem.* **269,** 23367–23373.
KRISHNASWAMY, S., FIELD, K. A., EDGINGTON, T. S., MORRISSEY, J. H. & MANN, K. G. (1992). Role of the membrane surface in the activation of human coagulation factor X. *J. Biol. Chem.* **267,** 26110–26120.
KRISHNASWAMY, S., NESHEIM, M. E., PRYZDIAL, E. L. G. & MANN, K. G. (1993). Assembly of the prothrombinase complex. *Methods Enzymol.* **222,** 260–280.
LOLLAR, P., KNUTSON, G. J. & FASS, D. N. (1985). Activation of protein factor VIII:C by thrombin & Factor Xa. *Biochemistry* **24,** 8056–8064.
MACFARLANE, R. G. (1964). An enzyme cascade in the blood clotting mechanism and its functions as a biological amplifier. *Nature* **202,** 498–499.
MANN, K. G., NESHEIM, M. E., CHURCH, W. R., HALEY, P. & KRISHNASWAMY, S. (1990). Surface-dependent reactions of the vitamin K-dependent enzyme complexes. *Blood* **76,** 1–16.
MANN, K. G. & LORAND, L. (1993). Introduction: blood coagulation. *Methods Enzymol.* **222,** 1–10.
MILETICH, P., JACKSON, C. M. & MAJERUS, P. W. (1977). Interaction of coagulation factor Xa with human platelets. *Proc. Natl. Acad. Sci. U.S.A.* **74,** 4033–4036.
MONKOVIC, D. D. & TRACY, P. B. (1990). Functional characterization of human platelet-released factor V and its activation by factor Xa and thrombin. *J. Biol. Chem.* **265,** 17132–17140.
MORRISSEY, J. H. (1995). Tissue factor modulation of factor VIIa activity: use in measuring trace levels of factor VIIa in plasma. *Thromb. Haemost.* **74,** 185–188.
MORTON, K. W. & MAYERS, D. F. (1994). *Numerical Solution of Partial Differential Equations*: *An Introduction*. New York: Cambridge University Press.
NEMERSON, Y. (1992). The tissue factor pathway of blood coagulation. *Semin. Haematol.* **29,** 170–176.
NESHEIM, M. E. & MANN, K. G. (1979). Thrombin-catalyzed activation of single chain bovine factor V. *J. Biol. Chem.* **254,** 1326–1334.
NESHEIM, M. E., TRACY, R. P. & MANN, K. G. (1984). 'Clotspeed', a mathematical simulation of the functional properties of prothrombinase. *J. Biol. Chem.* **259,** 1447–1453.
NESHEIM, M. E., TRACY, R. P., TRACY, P. B., BOSKOVIC, D. S. & MANN, K. G. (1992). Mathematical simulation of prothrombinase. *Methods Enzymol.* **215,** 316–328.
PEDERSEN, A. H., NORDFANG, O., NORRIS, F., WIBERG, F. C., CHRISTENSEN, P. M., MOELLER, K. B. *et al*. (1990). Recombinant human extrinsic pathway inhibitor. *J. Biol. Chem.* **265,** 16786–16793.
RADCLIFFE, R. & NEMERSON, Y. (1976). Mechanism of activation of bovine factor VII: products of cleavage by factor Xa. *J. Biol. Chem.* **251,** 4797–4802.
RAPAPORT, S. I. (1989). Inhibition of factor VIIa/tissue factor induced blood coagulation: with particular emphasis upon a factor Xa-dependent inhibitory mechanism. *Blood* **73,** 359–365.
ROSENBERG, R. D. & BAUER, K. A. (1994). The heparin–antithrombin system: a natural anticoagulant mechanism. In *Hemostasis and Thrombosis*: *Basic Principles and Clinical Practice*, 3rd Edn (Colman, R. W., Hirsh, J., Marder, V. J. & Salzman, E. W., eds), pp. 837–860. Philadelphia, PA: JB Lippincott Company.
ROSING, J., TANS, G., GOVERS-RIEMSLAG, W. P., ZWAAL, R. F. & HEMKER, H. C. (1980). The role of phospholipids and factor Va in the prothrombinase complex. *J. Biol. Chem.* **255,** 274–283.
SILVERBERG, S., NEMERSON, Y. & ZUR, M. (1977). Kinetics of the activation of bovine coagulation factor X by components of the extrinsic pathway. *J. Biol. Chem.* **252,** 8481–8488.
WILLEMS, G. M., LINDHOUT, T., HERMENS, W. T. & HEMKER, H. C. (1991). Simulation model for thrombin generation in plasma. *Haemostasis* **21,** 197–207.
YE, J. & ESMON, C. T. (1995). Factor Xa-Factor Va complex assembles in two dimensions with unexpected high affinity: an experimental and theoretical approach. *Biochemistry* **34,** 6448–6453.
ZUR, M. & NEMERSON, Y. (1980). Kinetics of factor IX activation via the extrinsic pathway. *J. Biol. Chem.* **255,** 5703–5707.

APPENDIX

Linearized Stability Analysis

Here we discuss the stability of solutions of the linearized system of eqns (22) with the matrix:

$$\mathbf{A} = \begin{pmatrix} -(a_1+k_{1in}) & a_2 & a_7 & 0 \\ a_1 & -(a_2+k_{1in}^m) & 0 & a_3 \\ a_8 & 0 & -(a_4+k_{2in}) & a_5 \\ 0 & a_6 & a_4 & -(a_5+k_{2in}^m) \end{pmatrix}. \tag{A.1}$$

For conciseness we have introduced the symbols

$$a_1 = k_{1on}(r_1^{Tv} - (z_1^{mv})^*) \quad a_4 = k_{2on}(r_2^{Tv} - (z_2^{mv})^*)$$
$$a_2 = k_{1off} \quad a_5 = k_{2off}$$
$$a_3 = \frac{k_{1cat}^m (z_1^{mv})^*}{K_{1M}^{mv} + (z_1^{\mathrm{mv}})^*} \quad a_6 = \frac{k_{2cat}^m (z_2^{mv})^*}{K_{2M}^{mv} + (z_2^{\mathrm{mv}})^*}$$
$$a_7 = \frac{k_{1cat} z_1^*}{K_{1M} + z_1^*} \quad a_8 = \frac{k_{2cat} z_2^*}{K_{2M} + z_2^*}. \tag{A.2}$$

Because eqn (22) is linear, its solutions are superpositions of exponentials in t with exponents $\lambda_k t$ for the four eigenvalues λ_k of the matrix $\mathbf{A}$. The perturbations decay if all of these eigenvalues have negative real part, and grow if one or more of the eigenvalues has positive real part. The eigenvalues are roots of the polynomial $p(\lambda) \equiv \det(A - \lambda I) = \lambda^4 + \alpha_3\lambda^3 + \alpha_2\lambda^2 + \alpha_1\lambda^1 + \alpha_0$. Here, the coefficients α_3, α_2, α_1, and α_0 depend on the kinetic parameters, the surface receptor densities, and the steady-state zymogen concentrations. A necessary and sufficient condition that all of the eigenvalues have negative real part is the Routh–Hurwitz condition: $\alpha_0 > 0$, $\alpha_1 > 0$, $\alpha_2 > 0$, $\alpha_3 > 0$, and $R \equiv \alpha_1\alpha_2\alpha_3 - \alpha_1^2 - \alpha_0\alpha_3^2 > 0$ (Edelstein-Keshet, 1988). So, if any of the coefficients α_i of $p(\lambda)$ is negative or if R is negative the system is linearly unstable and the small initial perturbations grow exponentially.

For Scenario 1 in which $a_7 = a_8 = 0$, we have shown that if $\alpha_0 > 0$, then also $\alpha_1 > 0$, $\alpha_2 > 0$, $\alpha_3 > 0$, and $R > 0$, and so the system is linearly stable. If $\alpha_0 < 0$, the system is linearly unstable. So the condition $\alpha_0 < 0$ gives a sharp threshold for the onset of instability. The coefficient α_0 equals the determinant of $\mathbf{A}$, and can be expressed in terms of the reaction rates $a_1, \ldots, a_6$ above, the inhibition rate k_{1in}, k_{1in}^m, k_{2in} and k_{2in}^m, and the binding equilibrium relations (21). The resulting expression gives inequality (23) as the stability condition.

For Scenario 2, the condition $\alpha_0 > 0$ by itself is no longer sufficient to ensure stability because enough enzymatic activity in either the solution phase or the membrane phase can destabilize the system. The inequality $\alpha_0 > 0$ in this scenario is:

$$\begin{aligned}&(k_{1in}^m(a_1 + k_{1in}) + k_{1in}k_{1off})(k_{2in}^m(a_4 + k_{2in}) \\ &+ k_{2in}k_{2off}) + (a_3a_6a_7a_8) > (a_1 + k_{1in}) \\ &\times (a_4 + k_{2in})(a_3a_6) + (k_{1off} + k_{1in}^m)(k_{2off} + k_{2in}^m) \\ &\times (a_7a_8) + a_1k_{2off}(a_6a_7) + a_4k_{1off}(a_3a_8)\end{aligned} \tag{A.3}$$

where a_1 and a_4 involve the unoccupied binding-site densities; a_3 and a_6 describe the membrane-bound enzyme activation rates; and a_7 and a_8 describe the solution-phase enzyme activation rates [see (A.2) above]. We have established the following results: if $\alpha_0 > 0$ and either of the inequalities (23) or

$$\begin{aligned}&\left(\frac{k_{1cat} z_1^*}{K_{1M} + z_1^*}\right)\left(\frac{k_{2cat} z_2^*}{K_{2M} + z_2^*}\right) \\ &< \left(k_{1in} + \frac{k_{1in}^m k_{1on}\left(1 - \frac{z_1^*}{K_{1D}^z + z_1^*}\right) r_1^{Tv}}{k_{1off} + k_{1in}^m}\right) \\ &\times \left(k_{2in} + \frac{k_{2in}^m k_{2on}\left(1 - \frac{z_2^*}{K_{2D}^z + z_2^*}\right) r_2^{Tv}}{k_{2off} + k_{2in}^m}\right)\end{aligned} \tag{A.4}$$

holds, then the other of these inequalities also holds, and the linearized system is stable. If $\alpha_0 < 0$, or if $\alpha_0 > 0$ and both of these inequalities are violated, then the linearized system is unstable. We note that in the case $k_{1cat} = 0$ and $k_{2cat} = 0$, condition (A.4) holds automatically and condition (A.3) reduces to condition (23) of Scenario 1.